Journal of Chromatography A 1769 (2026) 466702

Contents lists available at ScienceDirect

Journal of Chromatography A

journal homepage: www.elsevier.com/locate/chroma

Exploring adsorption–desorption kinetics and eddy dispersion in enantioselective hydrophilic interaction chromatography using teicoplanin-based chiral stationary phase☆

Chiara De Luca [a], Chiara Nosengo [a], Amirmohammad Faraji Shovey [a], Antonio Ricci [b], Martina Catani [a], Alberto Cavazzini [a,c], Fabrice Gritti [d], Simona Felletti [e,*]

[a] Dept. of Chemical, Pharmaceutical and Agricultural Sciences, University of Ferrara, via L. Borsari 46, 44121 Ferrara, Italy
[b] Fresenius Kabi iPSUM, via San Leonardo 23, Villadose (Rovigo), Italy
[c] Council for Agricultural Research and Economics, Via Della Navicella 2/4, 00184, Rome, Italy
[d] Waters Corporation, Core Research/Fundamental Milford, MA, 01757, USA
[e] Dept. of Environmental and Prevention Sciences, University of Ferrara, via L. Borsari 46, 44121 Ferrara, Italy

ARTICLE INFO

Keywords:
Adsorption–desorption kinetics
Chiral chromatography
Sub 2-μm fully porous particles
Ultrafast chiral separations

ABSTRACT

This research examined the kinetic behavior of two chiral probes (FMOC-Alanine and Haloxyfop) using a zwitterionic teicoplanin-based column and an aqueous-methanol mobile phase. More specifically, experimental results, supported by literature data measured using the same elution mode, indicate that the presence of a water layer adsorbed on the particle surface hinders analyte surface diffusion leading to localized adsorption. This shows cascading effects on longitudinal diffusion, solid–liquid mass transfer resistance and eddy dispersion, which become analyte-independent. The only difference in the measured plate heights is therefore given only by slow adsorption–desorption kinetics, confirming an important correlation between analyte structure and the extent of band broadening in chiral chromatography.

The findings reported in this study can be expanded to other molecules, suggesting that similar kinetic behavior could be expected if the same experimental conditions are maintained (e.g., same column manufacturer, silica particles, and elution mode). This would help accelerating the method development and the understanding of both the chiral recognition mechanism and the sources of band broadening occurring in chiral chromatography.

1. Introduction

Efficiency is one of the most important parameters in chromatography, usually calculated as the number of plate height (N) or the height equivalent to a theoretical plate, which is correlated to N through inverse proportionality ($H = L/N$, where L is the column length). These parameters estimate the "quality" of a separation in terms of peak width and symmetry. From a practical point of view, kinetic performance of a column can be evaluated by means of the well-known van Deemter equation, which correlate H to the variation of mobile phase flow rate. The optimum conditions for the separation (i.e., where efficiency is maximum) can be found at the minimum of the curve.

Nowadays, different solutions are developed by manufacturers to increase the efficiency of separations. The most popular approach consists in playing on the morphology of the stationary phase, either by reducing the particle diameter down to sub-2 μm range or by employing superficially porous particles (SPPs) [1–3]. Other advanced solutions have been also introduced into the market, including micropillar array columns, which have allowed a considerable step forward in efficiency especially for proteomics applications [4–6]. Nevertheless, while these considerations usually hold true in achiral separations, they cannot be taken for granted in chiral chromatography, where other variables have to be considered. Indeed, the enantiorecognition process (i.e., the ability of discriminating between two enantiomers) is the result of a series of multiple interactions, including hydrogen bonding, van der Waals and $\pi - \pi$ forces, hydrophobic, steric effects, ionic retention and repulsion effects [7–10], whose establishment is very difficult to be predicted. In addition, the surface of the adsorbent is usually heterogeneous, presenting both chiral (selective) sites, where the enantiorecognition actually takes place, and nonselective ones, such

☆ This article is part of a Special issue entitled: 'Fundamentals' published in Journal of Chromatography A.

* Corresponding author.
E-mail address: fllsmn1@unife.it (S. Felletti).

https://doi.org/10.1016/j.chroma.2026.466702
Received 31 October 2025; Received in revised form 7 January 2026; Accepted 9 January 2026
Available online 10 January 2026

as residual silanols, where the two enantiomers behave likewise. As a result, processes determining band broadening in an enantioseparation are more complicated than in achiral chromatography. Recent works have reported about the strong impact of adsorption–desorption kinetics which can be relevant especially for the more retained enantiomer at the point that its van Deemter curve appeared as convex-upward [11–16]. Despite various attempts reported over the years, the contribution of adsorption–desorption kinetics to band broadening is very difficult to be quantified. Another challenge is related to the fact that predicting when this contribution may arise is currently not possible, since it closely depends on the types of interactions that the two enantiomers establish with the stationary phase. Indeed, from a microscopic viewpoint, the slow adsorption–desorption kinetics is linked to a low probability of binding on the enantioselective site, because a very specific analyte-to-binding site chemical configuration is required, and this condition is rarely met statistically [17]. Moreover, to complicate further the things, it has to be taken into account that the way analytes bind with adsorption sites on the chiral selector is strictly dependent on the elution mode. It has been observed that enantiorecognition mechanism can be enhanced or hindered depending on the ability of the mobile phase components to interact with the chiral stationary phase (CSP). Clear examples, using polysaccharide-based CSP under polar organic mode (POM) conditions, are reported by Peluso and Shedania [18–20], where the use of acetonitrile, an aprotic solvent, favors analyte-selector interactions, while methanol, a protic solvent, being able to form H-bonds with the CSP, drastically reduces retention and enantioselectivity. On the other hand, studies with teicoplanin- and aglycone-based CSPs operated using aqueous-organic mobile phases revealed that compounds bearing COO^- group (the key fragment for interaction with the aglycone basket of CSPs, see Fig. 1) show enhanced retention and enantioselectivity using methanol-rich mobile phase compared to the acetonitrile-rich one [8,10,21–23]. This behavior could be ascribed to the multimodal and mixed-mode properties of these CSPs combined to the reduced number of water molecules adsorbed on the surface of the particles when using methanol-rich mobile phase [21], behaving like hydrophilic interaction liquid chromatography (HILIC). Indeed, the strong ability of methanol to form hydrogen bond reduces the interaction between water and the surface of the particles, which in turn decrease the adsorption competition with analytes leading to increased retention and selectivity. Hence, in this case, a partitioning-based retention mechanism could be limited in comparison to an adsorption-based one [7,8,21–25].

The use of methanol-rich mobile phases combined with the thermodynamically strong and enantioselective interaction between D-amino acids and these CSPs leads, in some cases, to an appreciable loss in efficiency, possibly related to a slow adsorption–desorption process between analyte and selector [7,21,22,26].

With the aim of expanding the current understanding on this matter, this work reports on the investigation of kinetic parameters affecting retention and band broadening of two different chiral analytes on a teicoplanin-based CSP, using a mixture of methanol/water 85/15% (v/v) as mobile phase. The chiral probes are FMOC-Alanine and Haloxyfop (structures in Fig. 2), both bearing a carboxylated group on their structure, which is fundamental to establish multiple H-bonds with the aglycone basket of the teicoplanin selector, as demonstrated through X-ray and molecular modeling investigations [7,8,22,27]. If compared to Haloxyfop, FMOC-Alanine can establish an additional H-bond with the selector through the amide NH group, contributing to stabilize the analyte/teicoplanin complex [2,7,8,21,22,28–31]. The effect of this more stereospecific interaction on the overall efficiency, and most importantly, on the adsorption desorption kinetics, will be evaluated in order to understand if it is possible to draw up some general considerations between specific analyte-CSP interactions and the occurrence of considerable effects of adsorption–desorption kinetics.

For a better readibility, a list of symbols is reported at the end of the article.

2. Theory

van Deemter equation is commonly used to evaluate kinetic performance of a chromatographic column. This equation accounts for all the non-equilibrium contributions given by eddy dispersion ($a(\nu)$), longitudinal diffusion (b), the solid–liquid mass transfer resistance due to the finite diffusivity of the analyte across the particle volume (c_p) and the adsorption–desorption kinetics due to a low probability of binding on the enantioselective site (c_{ads}) [32]. In reduced coordinates, for the two enantiomers ($i = 1,2$), it is written as:

$$h_i = a_i(\nu) + \frac{b_i}{\nu} + (c_{p,i} + c_{ads,i})\nu \tag{1}$$

with h the reduced plate height and ν the reduced interstitial velocity, defined as:

$$\nu = \frac{u_e\, d_p}{D_m} \tag{2}$$

with D_m the bulk molecular diffusion coefficient and u_e ($= F_v/\pi r_c^2 \epsilon_e$, being F_v the flow rate, r_c the column radius and ϵ_e the external column porosity) is the interstitial velocity, i.e. the velocity of the mobile phase moving between particles [33].

The first term appearing in Eq. (1) is the eddy dispersion, $a(\nu)$. This source of band broadening is related to bed heterogeneity which creates flow unevenness (velocity variation) in the column. These velocity biases arise on specific lengths, leading to a sum of different contributions commonly referred to as trans-channel, trans-column and inter-channel eddy dispersion [34]. $a(\nu)$ can then be written for the two enantiomers ($i = 1,2$):

$$a_i(\nu) = h_{TS,i} + h_{TC,i} + h_{SR,i} \tag{3}$$

where h_{TS} is the trans-channel contribution, where the velocity bias occurs between two adjacent particles, h_{TC} is the trans-column eddy dispersion, characterized by a distance equal to the column inner radius, and h_{SR} is the short-range inter-channel eddy dispersion, with a distance of a few particle diameters [32,35,36].

The use of stop-flow measurements, like peak parking (PP), permits to evaluate both effective and molecular diffusion coefficients, D_{eff} and D_m, respectively. For further details about PP method the reader is referred to [32,37,38]. Once these coefficients are known, the b term of Eq. (1) can be calculated for the first and the second eluted enantiomer ($i = 1,2$):

$$b_i = 2(1 + k_{1,i})\frac{D_{eff,i}}{D_m} = 2(1 + k_{1,i})\gamma_{eff,i} \tag{4}$$

with $k_{1,i}$ the zone retention factor (i.e. the retention factor referred to the interstitial volume [39–41]) of the ith enantiomer and $\gamma_{eff} = D_{eff}/D_m$ is the reduced effective diffusion coefficient.

The interpretation of D_{eff} can be done through diffusion models. Among all, the Torquato model can provide accurate estimation of diffusion coefficients since it takes into account the microstructure of packed beds and it is designed for random sphere packings in physical contact [32,42,43]:

$$D_{eff,i} = \frac{1}{\epsilon_e(1 + k_{1,i})}\left[\frac{1 + 2(1 - \epsilon_e)\beta_i - 2\epsilon_e\xi_2\beta_i^2}{1 - (1 - \epsilon_e)\beta_i - 2\epsilon_e\xi_2\beta_i^2}\right] D_m \tag{5}$$

with β_i defined as:

$$\beta_i = \frac{\Omega_i - 1}{\Omega_i + 2} \tag{6}$$

$\xi_2 = 0.3$ when particles are in physical contact. From Eq. (5) and (6), Ω can be derived. Ω is defined as the ratio between the effective diffusion coefficient through the porous particle ($D_{p,i}$) by considering the concentration gradient in the bulk phase and that in the bulk (D_m). Then the estimation of the trans-particle mass transfer resistance term, c_p, is possible through [44]:

$$c_{p,i} = \frac{1}{30}\frac{\epsilon_e}{1 - \epsilon_e}\left(\frac{k_{1,i}}{1 + k_{1,i}}\right)^2 \frac{1}{\Omega_i} \tag{7}$$

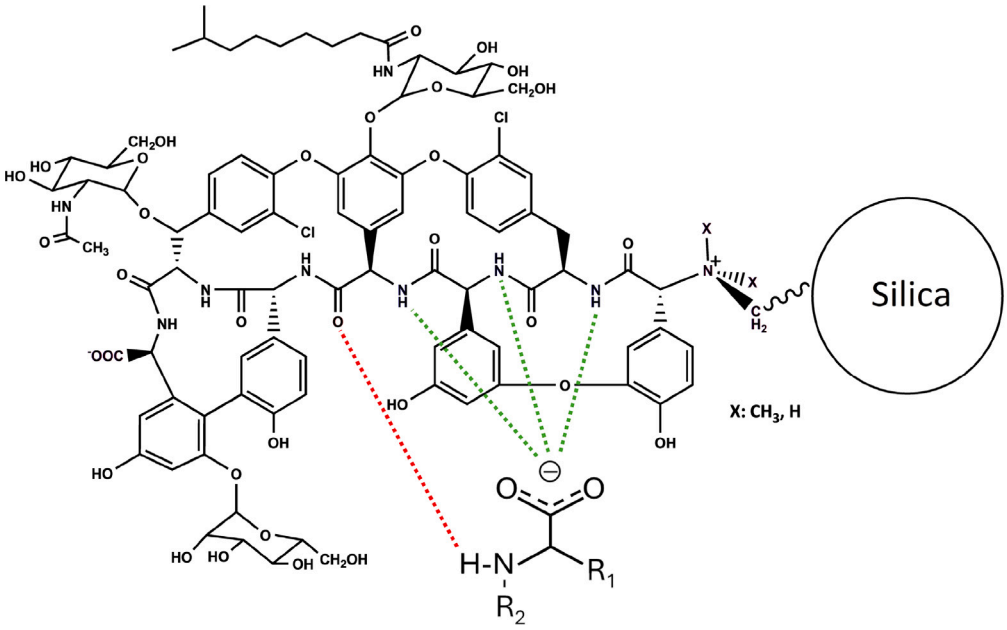

Fig. 1. 2D structure of zwitterionic teicoplanin chiral selector and a generic N-protected amino acid. Green dotted lines represent H-bonds between analyte carboxylate group and backbone amide NHs atoms; red dotted line indicates an additional H-bond between the carbonyl O atom of the CSP and the amide NH atom of the analyte [7].

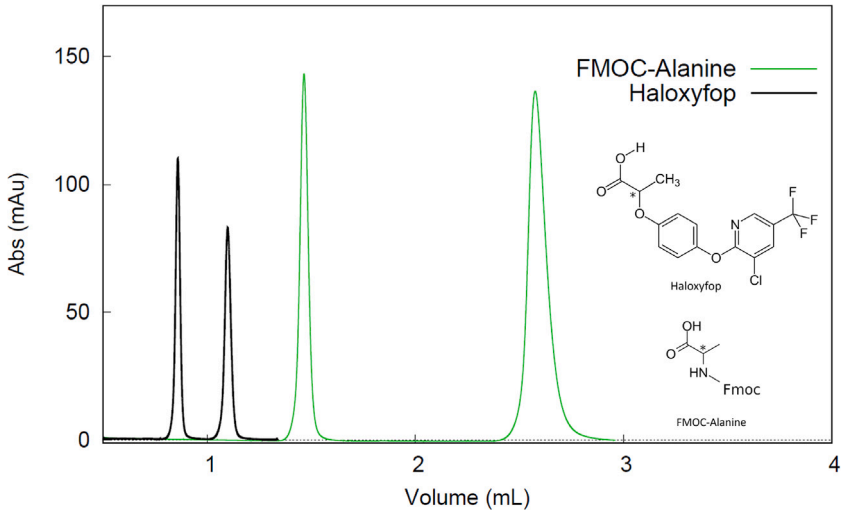

Fig. 2. Chromatogram of FMOC-Alanine (green) and Haloxyfop (black) enantiomers measured on a 50 × 3.0 mm column packed with zwitterionic teicoplanin stationary phase, 1.9 μm fully porous particles, flow rate = 0.2 ml/min, mobile phase = methanol/H_2O 85:15%(v/v) + 20 mM ammonium formate, injection volume =1 μl.

Concerning chiral separations, the complex phenomenon of chiral recognition and interaction between analyte and selector may not be instantaneous, as it commonly happens in achiral chromatography for small molecules. This leads to an additional source of band broadening due to the (slow) process of adsorption–desorption kinetics which cannot be neglected ($c_{ads} \neq 0$) [1,32,45,46]. c_{ads} is defined as:

$$c_{ads,i} = 2\,\frac{\epsilon_e}{1-\epsilon_e}\,\frac{1}{1-\epsilon_p}\left(\frac{k_{1,i}}{1+k_{1,i}}\right)^2\left(\frac{k_{p,i}}{1+k_{p,i}}\right)^2\frac{D_m}{k_{ads,i}d_p^2} \tag{8}$$

with k_{ads} the kinetic adsorption constant, $k_p = (1-\epsilon_p)K_a/\epsilon_p$, where ϵ_p is the internal porosity of the particle and K_a is the Henry's constant. k_1 and K_a are related through [32,35,47]:

$$k_1 = \frac{1-\epsilon_e}{\epsilon_e}\left[\epsilon_p + (1-\epsilon_p)K_a\right] \tag{9}$$

The estimation of c_{ads} is particularly important to better understand the modalities in which the enantiorecognition mechanism takes place and the strength of the interaction. This information is pivotal to develop new packing materials able to provide (ultra)high performance even at high flow rates, when the contribution of $c_p + c_{ads}$ becomes the most relevant. Nevertheless, accessing the c_{ads} is not straightforward, since all other contributions to band broadening reported in Eq. (1) must be known, i.e. $a(v)$, b and c_p, or k_{ads} must be quantified. Among them, only b and c_p can be directly accessed through PP (Eqs. (4), (7)). Hence, the commonly applied subtraction method to the overall h leads to the sum of the $a(v) + c_{ads}v$ contributions:

$$a_i(v) + c_{ads,i}v = h_i - \frac{b_i}{v} - c_{p,i}v \tag{10}$$

Over the years, different approaches have been proposed for the measurement of $a(v)$ and k_{ads} [17,31,32,35,36,45,48–53]. However,

different assumptions must be taken for granted and the need of performing theoretical computer simulations or additional experimental work make the application of these methods challenging, time-consuming and not generally applicable. Moreover, despite several works focused on the evaluation and calculation of the eddy dispersion contribution under reversed phase (RP) elution conditions have recently been published [36,51–53], showing a clear dependence on the retention factor, there is still a lack of studies about HILIC elution.

In this context, in this work, the integration of literature data and experimental results, measured under the same elution conditions, made possible the investigation of all the sources of band broadening, including c_{ads}, for two probe racemates (Fig. 2), one bearing only the COOH group (Haloxyfop) and one bearing both NH and COOH groups (FMOC-Alanine).

This study demonstrates that, if the chiral recognition mechanism has been fully understood, the kinetic behavior of a molecule can be translated to other similar molecules.

3. Experimental section

3.1. Columns and materials

All solvents, reagents and analytes (FMOC-D-Alanine, FMOC-L-Alanine and racemic Haloxyfop) were purchased from Merck Sigma-Aldrich (St. Louis, MO, USA). Fully porous silica particles of narrow particle size distribution (pore size 120 Å, particle size 1.9 μm and specific surface area 282 m^2/g) and teicoplanin chiral selector (Merck Sigma-Aldrich, St. Louis, MO, USA) were used to prepare the column under study. Particles total porosity (ϵ_t = 0.63), external porosity (ϵ_e = 0.38) and particle porosity (ϵ_p = 0.40) have been experimentally determined through Inverse Size Exclusion Chromatography [54]. Teicoplanin-based chiral stationary phase (CSP) was prepared as reported in Refs. [2,7] using a proprietary bonding protocol to immobilize the selector onto 1.9 μm porous particles, leading to the zwitterionic version (see Fig. 1). This CSP was then slurry packed into 50 × 3.0 mm empty stainless steel column, from IsoBar Systems by Idex (Erlangen, Germany). A 33 × 4.6 mm Micra column (Eprogen, Inc., USA) packed with 1.5 μm non-porous silica particles was from DBA Italia s.r.l. (Italy) and employed for the estimation of bulk molecular diffusion coefficients. The mobile phase was a mixture of methanol/H_2O 85:15%(v/v) + 20 mM ammonium formate.

3.2. Equipment

An UltiMate 3000 RS UHPLC chromatographic system from Thermo Fisher Dionex, consisting of a dual gradient RS pump, an in-line split loop well plate sampler, a thermostated RS column compartment and a diode array detector with a low dispersion 2.5 μL flow cell, was used. Detection wavelength was 214 nm. Two 350 × 0.10 mm I.D. Viper capillaries were used to connect the injector to the column and the column to the detector. The extra-column peak variance was 4.0 μL^2 at 1.0 mL/min.

van Deemter curves were measured by changing the flow rate from 0.05 to 1.5 mL/min. Peak parking was carried out at a flow rate of 0.2 mL/min. Injection volume was 1 μL and temperature was set to 35 °C.

4. Results and discussion

Chromatograms and chemical structures of the analytes are reported in Fig. 2. Table 1 reports zone retention factors ($k_{1,i}$) and selectivity ($\alpha = k_{1,2}/k_{1,1}$) values. As it can be noticed, retention and selectivity of FMOC-Alanine enantiomers are larger than Haloxyfop enantiomers. This can be attributed to a combination of steric fit and more specific and strong interactions between analyte and selector due to the simultaneous presence of COOH and NH groups [21].

In the following, the effects of the analyte structure on column performance will be discussed in detail.

4.1. van Deemter curves

van Deemter curves of FMOC-Alanine and Haloxyfop enantiomers are reported in Fig. 3. The curves measured for FMOC-Alanine present a larger gap between the two enantiomers if compared to Haloxyfop. The gap becomes more relevant at high interstitial velocities, where the contribution of the c-branch to the overall efficiency is prevailing. More in detail, the difference between the two curves ($h_2 - h_1$) measured at the highest ν for Haloxyfop enantiomers is only ~3 (ν_{max} = 28), while it is ~20 for FMOC-Alanine enantiomers (ν_{max} = 26). Interestingly, the slope of the curve of the first eluting enantiomer of FMOC-Alanine (L-Alanine) is very similar to those of Haloxyfop enantiomers, while the curve of the most retained FMOC-Alanine enantiomer (D-Alanine) is steeper. This may be an indicator of the stronger binding and slower adsorption–desorption process for the latter analyte. Conversely, in the region when the b term is prevailing (at small ν), the curves of both analytes follow the same trend, with similar efficiency values. Moreover, curves of both Haloxyfop and L-Alanine enantiomers are almost perfectly superimposed. In this context, longitudinal diffusion coefficients were estimated though the application of peak parking method and Eq. (4) to deeply understand the effect of the analyte structure on efficiency. Results show that the calculated b terms for the four enantiomers can be considered the same, with a value around 2.1 (see Table 1). This last trend was already observed on the same CSPs for other analytes [7,21,28,31] under various elution modes. In Refs. [21,31,55] it has been demonstrated that in cases where $b_1 = b_2$, the stationary phase diffusion is negligible, indicating that adsorption is localized. For these conditions, b values should be comparable for different analytes on the same column. To further confirm this finding, van Deemter curves of different analytes (including an achiral probe) measured on 50 × 3.0 mm and 100 × 4.6 mm teicoplanin columns packed with the same particle formats (fully porous, pore size 120 Å, particle size 1.9 μm, specific surface area 282 m^2/g) using MeOH/H_2O and ACN/H_2O 85:15% (v/v) + 20 mM ammonium formate mobile phases have been overlapped and are shown in Fig. S1. As it can be noted, all the curves coincide at small interstitial velocities (i.e. where longitudinal diffusion contribution is maximum), independently from both the analyte structure and the mobile phase composition. As a matter of fact, b = 2.0 was found for Z-D,L-Methionine enantiomers on a 100 × 4.6 mm teicoplanin column using ACN/H_2O as mobile phase [31]. From a mathematical viewpoint, the application of the Torquato model (Eq. (5)) to Eq. (4) leads to a retention-independent expression, indicating the β parameter, and hence Ω (see Eq. (6)), as the sole contribution to the b-term. As a matter of fact, only slight variations in Ω = 0.152 ± 0.005 have been observed between the four enantiomers under study, indicating very similar contributions to diffusion. From a physical viewpoint, this phenomenon of similar longitudinal diffusion is not unusual when an adsorbed layer of water is present on the surface of the stationary phase, especially under HILIC conditions [31,56–58]. In this context, it has been demonstrated in [21] that teicoplanin selectors, given their multiple interaction sites, exhibit a HILIC-like behavior, showing an excess of adsorbed water molecules, using both ACN/H_2O and MeOH/H_2O as mobile phases. In these cases, the analyte mobility in the water-rich layer (partition) and in adsorption sites (adsorption) is drastically reduced if compared to the bulk diffusion, leading to very close b/ν terms in the region where natural diffusion controls mass transfer (small ν).

As expected, c_p slightly increases with increasing retention, conversely to RP chromatography [57]. However, also in this case, given the very small variation of the Ω parameter between the four enantiomers, it can be stated that surface diffusion has an almost negligible influence on c_p.

Table 1
Zone retention factor (k_1), selectivity (α), bulk molecular diffusion coefficient (D_m), reduced effective diffusion coefficient (γ_{eff}), reduced longitudinal diffusion coefficient (b), reduced solid–liquid mass transfer resistance coefficient (c_p) measured on 1.9 μm teicoplanin-based chiral particles. 1st refers to the less retained enantiomer and 2nd refers to the most retained enantiomer.

Analyte	k_1		α	$D_m \times 10^{-6}$	γ_{eff}		b		c_p	
	1st	2nd		[cm^2/s]	1st	2nd	1st	2nd	1st	2nd
Haloxyfop	5.43	7.23	1.3	6.35	0.17	0.13	2.14	2.12	0.095	0.106
FMOC-Alanine	9.99	18.34	1.8	6.93	0.10	0.06	2.17	2.13	0.104	0.120

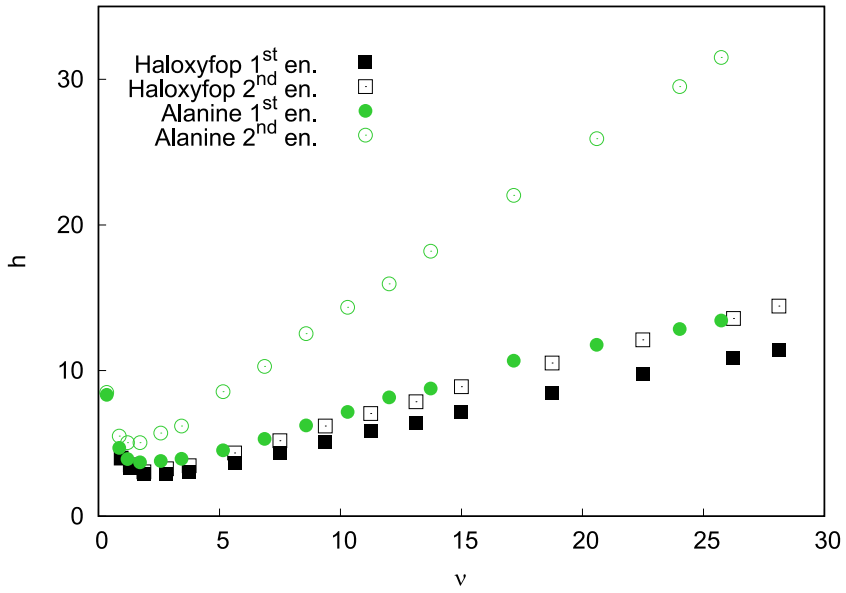

Fig. 3. Reduced van Deemter curves of first (full symbols) and second (empty symbols) eluted FMOC-Alanine (green) and Haloxyfop (black) enantiomers. Flow rates were changed in the range 0.05–1.5 mL/min.

4.2. Investigation of eddy dispersion and adsorption–desorption kinetics

Following the results reported in Section 4.1 and in Table 1, it can be stated that the contributions of longitudinal diffusion and the solid–liquid mass transfer resistance to the overall efficiency can be considered analyte-independent. Hence, to better understand the origin of the observed differences in the plate height between the two compounds (Fig. 3), a more detailed investigation of eddy dispersion and adsorption–desorption kinetics is required.

The subtraction of b and c_p terms to h, leading to the sum of $a(\nu) + c_{ads}\nu$ (Eq. (10)), has been performed and is graphically shown in Fig. 4. From this figure, the similar contribution of c_p to h for the entire set of molecules can be observed. Indeed, the gap between the curves of the two enantiomers $((a_2(\nu)+c_{ads,2}\nu)-(a_1(\nu)+c_{ads,1}\nu))$ is still ~20 for FMOC-Alanine and ~3 for Haloxyfop at ν_{max}, as observed for the total van Deemter curves ($h_2 - h_1$) reported in Section 4.1.

Concerning eddy dispersion, it is worth mentioning that this term is given by the sum of three contributions, accounting for three velocity biases characterized by a defined length: trans-channel (distance between two particles), short-range inter-channel (a few particle diameters) and trans-column (column radius) eddy dispersions (Eq. (3)) [32,35,52,53,56,57]. Despite many efforts over the years, the overall $a(\nu)$ term is still obtained empirically through experimental data (subtraction method) rather than with theoretical calculations, which require simplifying assumptions that may not correctly describe the real randomly packed beds [32,45,51–53]. Similar limitations are found for the estimation of the c_{ads} term [31,35,48,59]. Nevertheless, some insights on eddy dispersion can be obtained from data measured under HILIC conditions for achiral species reported in literature combined to the findings of this study, i.e. equal b, negligible surface diffusion, random packing. In particular, concerning the short-range inter-channel eddy dispersion, h_{SR}, it has been observed that it barely changes with retention (using k = 0.75–8.00), since the intra-particle diffusivity is practically constant [57]. Indeed, according to the formalism of Giddings, h_{SR} for porous particles is given by [57,60]:

$$h_{SR} = \frac{1}{\frac{b}{2\omega_{SR}\nu} + \frac{1}{2\lambda_{SR}}} \tag{11}$$

ω_{SR} and λ_{SR} parameters can be derived through the numerical resolution of the Navier–Stokes equation and by simulating advection-diffusion transport process using randomly packed non-porous particles ($b = 2\gamma_{eff}$). Since ω_{SR} and λ_{SR} are column geometrical parameters [35], h_{SR} is only governed by diffusion (γ_{eff}). In this work, only one stationary phase has been used and very similar γ_{eff}-terms have been calculated for the probes under study (Table 1), hence similar inter-channel eddy dispersion contributions are expected.

With the same philosophy, the influence of trans-column eddy dispersion and border effects (h_{TC}), due to column structural heterogeneity and the presence of column inlet and outlet, can be evaluated following Refs. [56,57,61]. It has to be stated that short and wide columns, as the one used in this study (50 × 3.0 mm), prevent the full radial equilibration of trans-column concentration gradients that are generated during analyte axial migration, leading to an increase in column efficiency if compared to long and narrow-bore columns [57,60,61]. Indeed, the analyte does not sample all the different flow paths across the column diameter, since the column radius is longer than the analyte radial excursion length, leading to a lower transient axial dispersion coefficient if compared to the asymptotic axial dispersion coefficient. However, for the same column dimensions, border effects cannot be neglected, due to the small intra-particle diffusivity of the analytes. The relaxation of radial concentration gradients, that originate at the column inlet and outlet, is indeed hindered by the too small transverse dispersion coefficient and the too large column diameter. In

Table 2
Adsorption–desorption kinetics coefficient (c_{ads}) and kinetic adsorption constants (k_{ads}) measured on 1.9 μm teicoplanin-based chiral particles.

Analyte	c_{ads}		k_{ads} [s^{-1}]	
	1st	2nd	1st	2nd
Haloxyfop	0.27	0.35	729	644
FMOC-Alanine	0.36	1.01	773	320

this context, a useful physical parameter related to the pre-asymptotic axial dispersion regime is the standard deviation of the radial position of the analyte, r, at the column outlet, defined as [57,61]:

$$r = 2\sqrt{\frac{Ld_p}{v}\left(\frac{b}{2} + 0.133v^{0.782}\right)} \tag{12}$$

Also in this case, the same considerations as for h_{SR} can be made, since r depends on both geometrical column parameters and the longitudinal diffusion. As reported in Fig. S2, r is practically independent from the retention factor of the analytes, as demonstrated in Refs. [56, 57] for HILIC separations.

The last contribution to the overall eddy dispersion is the trans-channel eddy dispersion, h_{TS}. This term, k-independent for random sphere packings and non-porous particles, is related to velocity biases at the boundary between the bulk mobile phase and the surface of adjacent porous particles. h_{TS} can be estimated as [17,32,62]:

$$h_{TS} = \frac{1}{\frac{1}{0.9} + \frac{1}{0.0045v}} \tag{13}$$

Based on these data, the observed differences in Fig. 4 could be only ascribed to differences in adsorption–desorption kinetics. The extent of the c_{ads} term can be evaluated through the fitting of the curves at high v values (v >13), where eddy dispersion tends to a constant value, as reported in various works [32,62–64]. Fitting results are graphically reported in Fig. S3. Not surprisingly (see Eq. (8)), the fitting of the four curves led to k-dependent results, obtaining curve slopes of 1.01 and 0.36 for the most and less retained FMOC-Alanine enantiomers and of 0.35 and 0.27 for Haloxyfop enantiomers (Table 2). From these c_{ads} values, kinetic adsorption constants (k_{ads}) can be estimated through Eq. (8) and are listed in Table 2. As expected, most retained enantiomers show smaller frequency of adsorption–desorption steps if compared to less retained ones. Moreover, very close values for firstly eluted enantiomers of both species have been observed. Interestingly, only a small difference is observed for Haloxyfop enantiomers (729 and 644 s^{-1}); in contrast the less retained FMOC-L-Alanine enantiomer shows more than 2 times higher k_{ads} than the other enantiomer (773 and 320 s^{-1}). For a direct comparison, compounds characterized by a fast adsorption–desorption kinetics show k_{ads} values as high as 10^7 s^{-1} [17,45], i.e. 5 orders of magnitude larger. The values reported in Table 2 confirm that FMOC-Alanine is able to better interact with the chiral selector. This is due to the combination of steric fit and the ability to form multiple H-bonds through both COOH and NH groups, which leads to a slower adsorption–desorption process that causes a big loss of efficiency, especially for the most retained enantiomer. Conversely, the presence of the sole carboxylate group in the Haloxyfop structure leads to weaker interactions with the chiral selector. This is then translated to a faster adsorption–desorption kinetics, which results in a smaller gap between the curves of first and second eluted enantiomer.

To further demonstrate these findings, all the measured sources of band broadening, namely b/v, $c_p v$ and $c_{ads} v$, have been subtracted to h, leading to the sole $a(v)$ contribution, reported in Fig. 5. As expected, differences in the eddy dispersion curves for the four compounds are negligible, demonstrating that the $a(v)$-term is k-independent under these experimental conditions, conversely to RP elution mode, where a clear dependence on retention has been observed [36,45,52,53,56].

List of symbols

Roman letters	
$a(v)$	reduced eddy diffusion plate height
b	reduced longitudinal diffusion coefficient
c_{ads}	reduced solid–liquid mass transfer resistance coefficient due to a slow adsorption–desorption process
c_p	reduced solid–liquid mass transfer resistance coefficient due to the finite rate of diffusion across the particle
D_p	effective sample diffusivity across the particle (cm^2/s)
D_{eff}	effective diffusion coefficient of the packed bed (cm^2/s)
d_p	average particle diameter (cm)
D_m	bulk molecular diffusion coefficient (cm^2/s)
F_v	flow rate (mL/min)
h	reduced plate height
h_{SR}	reduced short-range inter-channel eddy dispersion plate height
h_{TC}	reduced trans-column eddy dispersion plate height
h_{TS}	reduced trans-channel eddy dispersion plate height
H	plate height (μm)
i	1: first enantiomer, 2: second enantiomer
k	retention factor
k_1	zone retention factor
k_p	particle retention factor
k_{ads}	adsorption rate constant (s^{-1})
K_a	equilibrium Henry's constant
N	column efficiency
L	column length (mm)
r	standard deviation of the transverse excursion length (cm)
r_c	column inner radius (cm)
u_e	interstitial linear velocity (cm/s)
Greek letters	
α	chromatographic selectivity
β	parameter in Torquato's model of effective diffusion in packed beds
ϵ_e	external column porosity
ϵ_p	particle porosity
ϵ_t	total column porosity
γ_{eff}	reduced effective diffusion coefficient (D_{eff}/D_m)
ν	reduced interstitial linear velocity
Ω	ratio of the effective diffusivity of the sample in the porous particle to its bulk diffusion coefficient (D_p/D_m)
λ_{SR}	flow eddy dispersion coefficient related to short-range inter-channel velocity bias
ω_{SR}	diffusion eddy dispersion coefficient related to short-range inter-channel velocity bias
ξ_2	adjustable parameter in Torquato's model of effective diffusion in packed beds

To better visualize this outcome, the result of the deconvolution of the total h is reported in Fig. 6 for the four enantiomers, where the relative individual contribution of the four sources of band broadening (Eq. (1)) is presented. From this figure, the great impact of slow adsorption–desorption kinetics is clearly observed at height reduced interstitial velocity, where it accounts for more than 60% of the total reduced plate height for Haloxyfop and the less retained FMOC-L-Alanine enantiomer and for more than 80% for the most retained one.

5. Conclusions

In this study the kinetic behavior of two different chiral probes (FMOC-Alanine and Haloxyfop) with structural differences has been

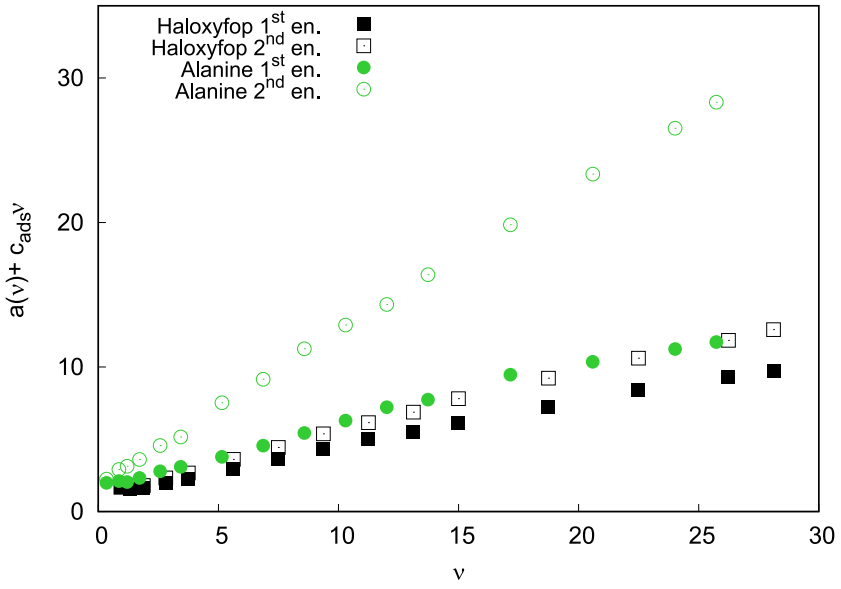

Fig. 4. Application of the subtraction method to the total plate height, Eq. (10), resulting in $a(\nu) + c_{ads}\nu$ contributions of first (full symbols) and second (empty symbols) eluted FMOC-Alanine (green) and Haloxyfop (black) enantiomers.

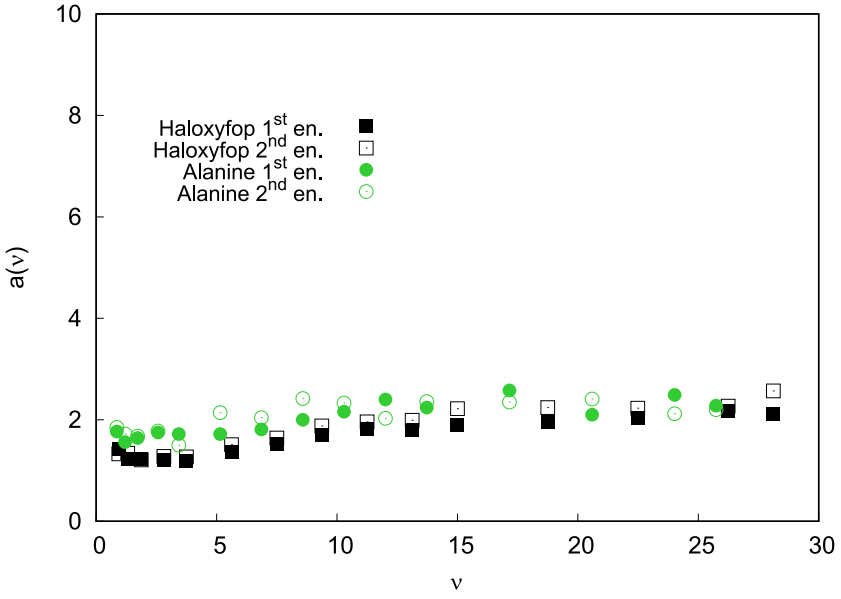

Fig. 5. Plots of eddy dispersion contributions for FMOC-Alanine (green) and Haloxyfop (black) enantiomers (full symbols: first enantiomer; empty symbols: second enantiomer).

investigated under HILIC-like conditions on a zwitterionic teicoplanin-based column.

More in details, it has been demonstrated that the most impacting source of band broadening is the slow adsorption–desorption process, which is directly correlated to retention of analytes and their adsorption rate constant. Conversely, other contributions to h, namely longitudinal diffusion, eddy dispersion and solid–liquid mass transfer resistance, can be considered analyte-independent.

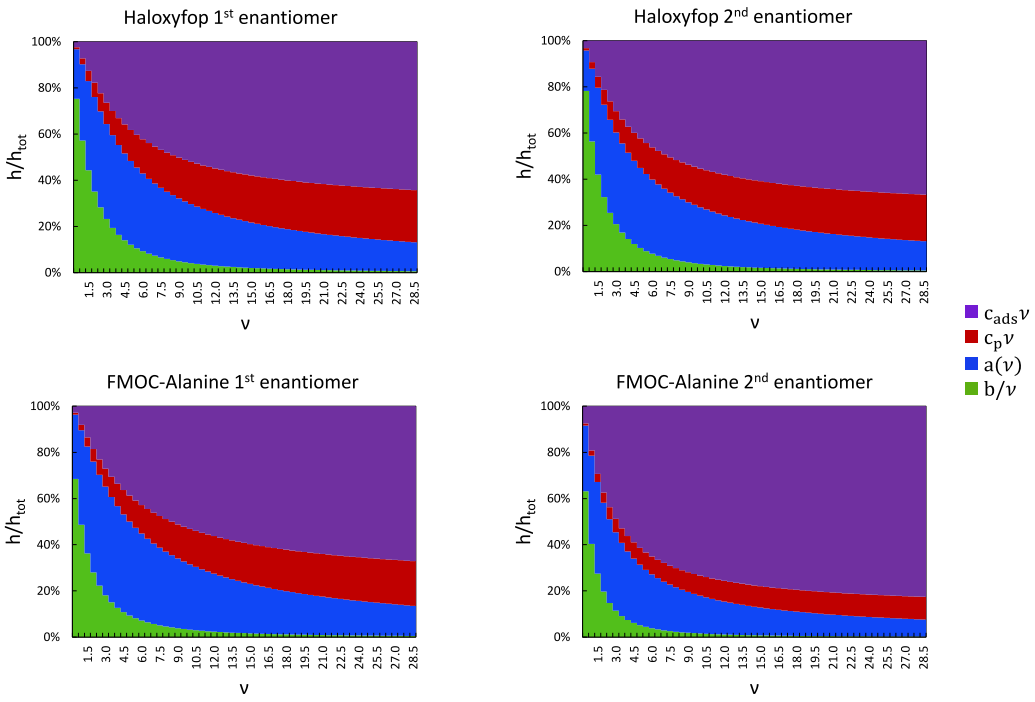

Fig. 6. Individual reduced plate height contributions (h, given by longitudinal diffusion b/ν in green, eddy dispersion $a(\nu)$ in blue, mass transfer resistance $c_p\nu$ in red, and adsorption–desorption kinetics $c_{ads}\nu$ in purple) to the total plate height (h_{tot}) obtained for the two racemic couples under study.

These results can contribute to draw a more general viewpoint on the specific interactions between chiral analytes and stationary phase under the complex and still not fully understood HILIC-like elution mode. Results of this work could be expanded to other molecules if the same experimental conditions are maintained (e.g. the same column manufacturer, the same silica, the same elution mode, etc.), avoiding the traditional time- and resource-consuming trial and error method.

CRediT authorship contribution statement

Chiara De Luca: Writing – original draft, Methodology, Formal analysis. **Chiara Nosengo:** Validation, Methodology, Investigation. **Amirmohammad Faraji Shovey:** Formal analysis, Data curation. **Antonio Ricci:** Supervision, Resources. **Martina Catani:** Supervision, Funding acquisition, Data curation. **Alberto Cavazzini:** Supervision, Project administration, Funding acquisition. **Fabrice Gritti:** Writing – review & editing, Supervision, Conceptualization. **Simona Felletti:** Writing – review & editing, Supervision, Conceptualization.

Declaration of competing interest

The authors declare that they have no known competing financial interests or personal relationships that could have appeared to influence the work reported in this paper.

Acknowledgments

The authors would like to thank the National Recovery and Resilience Plan (NRRP), Mission 04 Component 2 Investment 1.5 - NextGenerationEU, Call for tender n. 3277 dated 30/12/2021; Award Number: 0001052 dated 23/06/2022. The authors would also like to thank the Italian University and Scientific Research Ministry (grant P2022PTYWP, title: "Design of highpRofit fostEring bioActive coMpounds through integral valorization of seaWEEDs infesting the MEditerranean sea (DreamWEEDme)" and grant P2022AJA7H8, title "High revenue-generating molecules from industrial hemp: cost-effective, chemical classification-driven solutions for their production (CHempion)") as well as the Regional Programme of the European Regional Development Fund (PR FESR 2021–2027 Priority 1) project title "Production of high- added-value ingredients from fruit supply chain by-products through a cascade biorefinery approach - Frurefinery" for financial support.

Data availability

Data will be made available on request.

References

[1] M. Catani, S. Felletti, O.H. Ismail, F. Gasparrini, L. Pasti, N. Marchetti, C.D. Luca, V. Costa, A. Cavazzini, New frontiers and cutting edge applications in ultra high performance liquid chromatography through latest generation superficially porous particles with particular emphasis to the field of chiral separations, Anal. Bioanal. Chem. 410 (2018) 2457–2465.

[2] O.H. Ismail, M. Antonelli, A. Ciogli, C. Villani, A. Cavazzini, M. Catani, S. Felletti, D.S. Bell, F. Gasparrini, Future perspectives in high efficient and ultrafast chiral liquid chromatography through zwitterionic teicoplanin-based 2 μm superficially porous particles, J. Chromatogr. A 1520 (2017) 91–102.

[3] S. Felletti, C. De Luca, G. Lievore, L. Pasti, T. Chenet, G. Mazzoccanti, F. Gasparrini, A. Cavazzini, M. Catani, Investigation of mass transfer properties and kinetic performance of high-efficiency columns packed with c18 sub-2 μm fully and superficially porous particles, J. Sep. Sci. 43 (2020) 1737–1745.

[4] A. Moussa, B. Huygens, C. Venditti, A. Adrover, G. Desmet, Theoretical computation of the band broadening in micro-pillar array columns, J. Chromatogr. A 1715 (2024) 464607.

[5] H. Eghbali W. De Malsche, D. Clicq, J. Vangelooven, H. Gardeniers, G. Desmet, Pressure-driven reverse-phase liquid chromatography separations in ordered nonporous pillar array columns, Anal. Chem. 79 (2007) 5915–5926.

[6] B. Vankeerberghen, G. Desmet J. Op de Beeck, On-chip comparison of the performance of first- and second- generation micropillar array columns, Anal. Chem. 95 (2023) 13822–13828.

[7] O.H. Ismail, A. Ciogli, C. Villani, M.D. Martino, M. Pierini, A. Cavazzini, D.S. Bell, F. Gasparrini, Ultra-fast high-efficiency enantioseparations by means of a teicoplanin-based chiral stationary phase made on sub-2 μm totally porous silica particles of narrow size distribution, J. Chromatogr. A 1427 (2016) 55–68.

[8] A. Cavazzini, G. Nadalini, F. Dondi, F. Gasparrini, A. Ciogli, C. Villani, Study of mechanisms of chiral discrimination of amino acids and their derivatives on a teicoplanin-based chiral stationary phase, J. Chromatogr. A 1031 (2004) 143–158.

[9] I. Ilisz, R. Berkecz, A. Péter, Retention mechanism of high-performance liquid chromatographic enantioseparation on macrocyclicglycopeptide-based chiral stationary phases, J. Chromatogr. A 1216 (2009) 1845–1860.

[10] D.V. McCalley, Practical examination of flow rate effects and influence of the stationary phase water layer on peak shape and retention in hydrophilic interaction liquid chromatography, J. Chromatogr. A 1715 (2024) 464608.

[11] S. Felletti, M. Catani, G. Mazzoccanti, C.D. Luca, G. Lievore, A. Buratti, L. Pasti, F. Gasparrini, A. Cavazzini, Shedding light on mechanisms leading to convex-upward van Deemter curves on a cellulose tris(4-chloro-3-methylphenylcarbamate)-based chiral stationary phase, J. Chromatogr. A 1630 (2020) 461532.

[12] L.D. Asnin, A.A. Boteva, O.P. Krasnykh, M.V. Stepanova, I. Ali, Unusual van deemter plots of optical isomers on a chiral brush-type liquid chromatography column, J. Chromatogr. A 1592 (2019) 112–121.

[13] D.C. Patel, Z.S. Breitbach, M.F. Wahab, C.L. Barhate, D.W. Armstrong, Gone in seconds: praxis, performance and peculiarities of ultrafast chiral liquid chromatography with superficially porous particles, Anal. Chem. 87 (2015) 9137–9148.

[14] C.L. Barhate, Z.S. Breitbach, E.C. Pinto, E.L. Regalado, C.J. Welch, D.W. Armstrong, Ultrafast separation of fluorinated and desfluorinated pharmaceuticals using highly efficient and selective chiral selectors bonded to superficially porous particles, J. Chromatogr. A 1426 (2015) 241–247.

[15] S. Felletti, C.D. Luca, M. Catani, A. Cavazzini, Fundamental Kinetic Studies for Understanding Chiral Separations in High-Performance Liquid Chromatography, Springer, US, New York, NY, 2026, pp. 329–338, http://dx.doi.org/10.1007/978-1-0716-5023-3_16.

[16] S. Aslani, M.F. Wahab, M.E. Kenari, A. Berthod, D.W. Armstrong, An examination of the effects of water on normal phase enantioseparations, Anal. Chim. Acta (2022) 339608.

[17] D. Hlushkou, F. Gritti, A. Daneyko, G. Guiochon, U. Tallarek, How microscopic characteristics of the adsorption kinetics impact macroscale transport in chromatographic beds, J. Phys. Chem. C 117 (2013) 22974–22985.

[18] P. Peluso, B. Chankvetadze, The molecular bases of chiral recognition in 2-(benzylsulfinyl) benzamide enantioseparation, Anal. Chim. Acta 1141 (2021) 194–205.

[19] Z. Shedania, R. Kakava, A. Volonterio, T. Farkas, B. Chankvetadze, Separation of enantiomers of chiral sulfoxides in high-performance liquid chromatography with cellulose-based chiral selectors using methanol and methanol-water mixtures as mobile phases, J. Chromatogr. A 1557 (2018) 62–74.

[20] Z. Shedania, R. Kakava, A. Volonterio, T. Farkas, B. Chankvetadze, Separation of enantiomers of chiral sulfoxides in high-performance liquid chromatography with cellulose-based chiral selectors using acetonitrile and acetonitrile-water mixtures as mobile phases, J. Chromatogr. A 1609 (2020) 460445.

[21] S. Felletti, C. De Luca, G. Mazzoccanti, F. Gasparrini, S. Manetto, F.A. Franchina, T. Chenet, L. Pasti, A. Cavazzini, M. Catani, Understanding the transition from high-selective to high-efficient chiral separations by changing the organic modifier with zwitterionic-teicoplanin chiral stationary phase, Anal. Chem. 95 (2023) 9630–9637.

[22] A. Berthod, X.H. Chen, J.P. Kullman, D.W. Armstrong, F. Gasparrini, C. Villani I. D'Acquarica, A. Carotti, Role of the carbohydrate moities in chiral recognition on teicoplanin-based lc stationary phases, Anal. Chem. 72 (2000) 1767–1780.

[23] D. Tanács, R. Berkecz, A. Misicka, D. Tymecka, F. Fülöp, D.W. Armstrong, I. Ilisz, A. Péter, Enantioseparation of *beta*^{2}-amino acids by liquid chromatography using core–shell chiral stationary phases based on teicoplanin and teicoplanin aglycone, J. Chromatogr. A 1653 (2021) 462383.

[24] M. Liu, J. Ostovic, E.X. Chen, N. Cauchon, Hydrophilic interaction liquid chromatography with alcohol as a weak eluent, J. Chromatogr. A 1216 (2009) 2362–2370.

[25] Y. Guo, D. Muscatiello, An update on the progress in fundamental understanding of hydrophilic interaction liquid chromatography, J. Chromatogr. A 1765 (2026) 466520.

[26] A. Berthod, Y.B. Liu, C. Bagwill, D.W. Armstrong, Facile liquid chromatographic enantioresolution of native amino acids and peptides using a teicoplanin chiral stationary phase, J. Chromatogr. A 731 (1996) 123–137.

[27] S. Han, B. Le, H. Hajare, R. Baxter, S. Miller, X-ray crystal structure of teicoplanin a-2 bound to a catalytic peptide sequence via the carrier protein strategy, J. Org. Chem. 79 (2014) 8550–8556.

[28] O.H. Ismail, M. Catani, G. Mazzoccanti, S. Felletti, S. Manetto, C. De Luca, M. Ye, A. Cavazzini, F. Gasparrini, Boosting the enantioresolution of zwitterionic-teicoplanin chiral stationary phases by moving to wide-pore core–shell particles, J. Chromatogr. A 1676 (2022) 463190.

[29] O.H. Ismail, M. Antonelli, A. Ciogli, M. De Martino, M. Catani, C. Villani, A. Cavazzini, M. Ye, D.S. Bell, F. Gasparrini, Direct analysis of chiral active pharmaceutical ingredients and their counterions by ultra high performance liquid chromatography with macrocyclic glycopeptide-based chiral stationary phases, J. Chromatogr. A 1576 (2018) 42–50.

[30] P. Jander, A. Felinger V. Bačkovská, Analysis of the band profiles of the enantiomers of phenylglycine in liquid chromatography on bonded teicoplanin columns using the stochastic theory of chromatography, J. Chromatogr. A 919 (2001) 67–77.

[31] C. De Luca, G. Compagnin, C. Nosengo, G. Mazzoccanti, F. Gasparrini, A. Cavazzini, M. Catani, S. Felletti, Novel insights into the dependence of adsorption–desorption kinetics on particle geometry in chiral chromatography, Anal. Bioanal. Chem. 416 (2024) 1809–1820.

[32] F. Gritti, G. Guiochon, Mass transfer kinetics, band broadening and column efficiency, J. Chromatogr. A 1221 (2012) 2–40.

[33] U.D. Neue, HPLC Columns: Theory, Technology and Practice, Wiley-VCH, 1997.

[34] J.C. Giddings, H. Eyring, A molecular dynamic theory of chromatography, J. Phys. Chem. 59 (1955) 416–421.

[35] J.C. Giddings, Dynamics of Chromatography, Marcel Dekker, New York, 1965.

[36] G. Desmet, H. Song, D. Makey, D.R. Stoll, D. Cabooter, Experimental investigation of the retention factor dependency of eddy dispersion in packed bed columns and relation to knox's empirical model parameters, J. Chromatogr. A 1626 (2020) 461339.

[37] K. Miyabe, N. Ando, G. Guiochon, Peak parking method for measurement of molecular diffusivity in liquid phase systems, J. Chromatogr. A 1216 (2009) 4377–4382.

[38] K. Miyabe, Y. Matsumoto, G. Guiochon, Peak parking-moment analysis. A strategy for the study of the mass-transfer kinetics in the stationary phase, Anal. Chem. 79 (2007) 1970–1982.

[39] G. Desmet, K. Broeckhoven, J.D. Smet, S. Deridder, G.V. Baron, P. Gzil, Errors involved in the existing B-term expressions for the longitudinal diffusion in fully porous chromatographic media. Part I: Computational data in ordered pillar arrays and effective medium theory, J. Chromatogr. A 1188 (2008) 171–188.

[40] M. Catani, O.H. Ismail, F. Gasparrini, M. Antonelli, L. Pasti, N. Marchetti, S. Felletti, A. Cavazzini, Recent advancements and future directions of superficially porous chiral stationary phases for ultrafast high-performance enantioseparations, Analyst 142 (2017) 555–566.

[41] J.H. Knox, H.P. Scott, B and C terms in the van Deemter equation for liquid chromatography, J. Chromatogr. 282 (1983) 297–313.

[42] F. Gritti, G. Guiochon, General HETP equation for the study of mass-transfer mechanisms in RPLC, Anal. Chem. 78 (2006) 5329–5347.

[43] S. Torquato, Effective electrical conductivity of two-phase disordered composite media, J. Appl. Phys. 58 (1985) 3790–3797.

[44] K. Kaczmarski, G. Guiochon, Modeling of the mass-transfer kinetics in chromatographic columns packed with shell and pellicular particles, Anal. Chem. 79 (2007) 4648–4656.

[45] F. Gritti, G. Guiochon, Mass transfer mechanism in chiral reversed phase liquid chromatography, J. Chromatogr. A 1332 (2014) 35–45.

[46] L. Pasti, N. Marchetti, R. Guzzinati, M. Catani, V. Bosi, F. Dondi, A. Sepsey, A. Felinger, A. Cavazzini, Microscopic models of liquid chromatography: From ensemble-averaged information to resolution of fundamental viewpoint at single-molecule level, TrAC 81 (2016) 63–68.

[47] G. Guiochon, A. Felinger, D.G. Shirazi, A. Katti, Fundamentals of Preparative and Nonlinear Chromatography, second ed., Elsevier Academic Press, Amsterdam, 2006.

[48] A. Cavazzini, M. Remelli, F. Dondi, A. Felinger, Stochastic theory of multiple-site linear adsorption chromatography, Anal. Chem. 71 (1999) 3453–3462.

[49] A. Felinger, A. Cavazzini, M. Remelli, F. Dondi, Stochastic-dispersive theory of chromatography, Anal. Chem. 71 (1999) 4472–4479.

[50] A. Cavazzini, M. Remelli, F. Dondi, Stochastic theory of two-site adsorption chromatography by the characteristic function method, J. Microcol. Sep. 9 (1997) 295–302.

[51] B. Huygens, G. Desmet, A logarithmic law for the velocity- and retention-dependency of the eddy dispersion in chromatographic columns, J. Chromatogr. A 1730 (2024) 465088.

[52] F. Gritti, Mass transfer resistance in the mobile phase: Theory, data, and strategies to further improve the resolution power in pressure-driven liquid chromatography, J. Chromatogr. A 1760 (2025) 466289.

[53] U. Tallarek, D. Hlushkou, A. Höltzel, Multiscale simulation of liquid chromatography: Impact of retention on the plate height in packed beds, J. Chromatogr. A 1761 (2025) 466401.

[54] D. Cherrak M. Al-Bokari, G. Guiochon, Determination of the porosities of monolithic columns by inverse size-exclusion chromatography, J. Chromatogr. A 975 (2002) 275–284.

[55] S. Felletti, M. Catani, G. Mazzoccanti, C.D. Luca, G. Lievore, A. Buratti, L. Pasti, F. Gasparrini, A. Cavazzini, Mass transfer kinetics on modern Whelk-O1 chiral stationary phases made on fully- and superficially-porous particles, J. Chromatogr. A 1637 (2021) 461854.

[56] G. Gritti, G. Guiochon, Mass transfer mechanism in hydrophilic interaction chromatography, J. Chromatogr. A 1302 (2013) 55–64.

[57] G. Gritti, G. Guiochon, Comparison between the intra-particle diffusivity in the hydrophilic interaction chromatography and reversed phase liquid chromatography modes, Impact the Column Effic. J. Chromatogr. A 1297 (2013) 85–95.

[58] J.C. Heaton, D.V. McCalley, Comparison of the kinetic performance and retentivity of sub-2 μm core–shell, hybrid and conventional bare silica phases in hydrophilic interaction chromatography, J. Chromatogr. A 1371 (2014) 106–116.

[59] A. Felinger, A. Cavazzini, M. Remelli, F. Dondi, Stochastic-dispersive theory of chromatography, Anal. Chem. 71 (1999) 4472–4479.
[60] F. Gritti, G. Guiochon, Perspectives on the evolution of the column efficiency in liquid chromatography, Anal. Chem. 85 (2013) 3017–3035.
[61] A. Daneyko, S. Khirevich, A. Höltzel, A. Seidel-Morgenstern, U. Tallarek, From random sphere packings to regular pillar arrays: effect of the macroscopic confinement on hydrodynamic dispersion, J. Chromatogr. A 1257 (2012) 98–115.
[62] S. Khirevich, A. Daneyko, A. Höltzel, A. Seidel-Morgenstern, U. Tallarek, Statistical analysis of packed beds, the origin of short-range disorder, and its impact on eddy dispersion, J. Chromatogr. A 1217 (2010) 4713–4722.
[63] F. Gritti, G. Guiochon, Impact of retention on trans-column velocity biases in packed columns, AICHE J. 56 (2010) 1495–1509.
[64] F. Gritti, G. Guiochon, Relationship between trans-column eddy diffusion and retention in liquid chromatography: Theory and experimental evidence, J. Chromatogr. A 1217 (2010) 6350–6365.